Journal of Molecular Modeling (2023) 29:123
https://doi.org/10.1007/s00894-023-05530-7

ORIGINAL PAPER

Evaluation of autophagy inhibition to combat cancer: (vanadium complex)–protein interactions, parameterization, and validation of a new force field

Taináh M. R. Santos[1] · Camila A. Tavares[1] · Ander F. Pereira[2] · Elaine F. F. da Cunha[1] · Teodorico C. Ramalho[1,3]

Received: 29 September 2022 / Accepted: 23 March 2023 / Published online: 30 March 2023

Abstract
Autophagy has drawn attention from the scientific community, mainly because of its significant advantages over chemotherapeutic processes. One of these advantages is its direct action on cancer cells, avoiding possible side effects, unlike chemotherapy, which reaches tumor cells and affects healthy cells in the body, leading to a great loss in the quality of life of patients. In this way, it is known that vanadium complex (VC) [VO(oda)(phen)] has proven inhibition effect on autophagy process in pancreatic cancer cells. Keeping that in mind, molecular dynamics (MD) simulations can be considered excellent strategies to investigate the interaction of metal complexes and their biological targets. However, simulations of this type are strongly dependent on the appropriate choice of force field (FF). Therefore, this work proposes the development of AMBER FF parameters for VC, having a minimum energy structure as a starting point, obtained through DFT calculations with B3LYP/def2-TZVP level of theory plus ECP for the vanadium atom. An MD simulation in vacuum was performed to validate the developed FF. From the structural analyses, satisfying values of VC bond lengths and angles were obtained, where a good agreement with the experimental data and the quantum reference was found. The RMSD analysis showed an average of only 0.3%. Finally, we performed docking and MD (120 ns) simulations with explicit solvent between VC and PI3K. Overall, our findings encourage new parameterizations of metal complexes with significant biological applications, as well as allow to contribute to the elucidation of the complex process of autophagy.

Keywords AMBER force field · Vanadium complex · Molecular dynamics · Docking · Autophagy

Introduction

Without a doubt, COVID-19 (Coronavirus Disease 2019), caused by SARS-CoV-2 (severe acute respiratory syndrome coronavirus 2), has taken the place of the dreaded disease of the century [1]. However, until recently, this prominent place was taken by cancer. According to the most recent estimate, cancer killed about 10.0 million people in the year 2020, in addition to a total of 19.3 million new cases [2, 3].

Pancreatic cancer, also known as pancreatic ductal adenocarcinoma (PDAC), is among the most lethal cancers due to the aggressive nature of the tumor and late diagnosis [4–6]. It is estimated that in the year 2020, there were approximately 496,000 pancreatic cancer diagnoses and approximately 466,000 deaths were reported, amounting to 4.7% of cancer-related deaths worldwide [2].

The most up-to-date treatments are based on 5-fluorouracil or gemcitabine. However, these drugs offer only a brief survival period within months in the palliative care scenario [7]. Despite advances in the field, it can be said that there is no targeted therapy for pancreatic ductal adenocarcinoma, which leads to traditional treatments such as chemotherapy [8]. Nevertheless, despite aiming at eliminating cancer cells, chemotherapeutic processes end up also damaging perfectly

✉ Taináh M. R. Santos
tainah-martins@hotmail.com

✉ Teodorico C. Ramalho
teo@ufla.br

[1] Laboratory of Molecular Modelling, Department of Chemistry, Federal University of Lavras, /MG, Lavras 37200-000, Brazil

[2] Institute of Chemistry, University of Campinas, /SP, Campinas 13083-970, Brazil

[3] Department of Chemistry, Faculty of Science, University of Hradec Kralove, Hradec Kralove, Czech Republic

healthy cells and tissues, which induces side effects, leading to a drastic decrease in the quality of life of patients [9].

The limited effectiveness of this type of treatment, in addition to the increasing prevalence of drug-resistant tumors are strong arguments for seeking new treatment strategies. Thus, one of the most important challenges of modern scientific research is the pursue of new compounds that affect important processes in the development, progression, and metastasis of tumors [10, 11].

Keeping that in mind, the literature has increasingly highlighted an important process that can be a great ally in fighting cancer, which is the processes of autophagy [12]. Autophagy has shown itself to be a growing field in science, mainly because it has recently been highlighted by the recognition of the contributions of Dr. Yoshinori Ohsumi, 2016 Nobel Prize laureate in Medicine or Physiology [13].

Autophagy (or macroautophagy) consists of cell recycling mechanism, where materials, such as damaged organelles and malformed proteins, are taken to the lysosome for the degradation of the damaged materials to occur [14–16]. Its process starts when undue contents in the cytosol are encompassed by a membrane known as phagophore [17]. When this phagophore elongates, the autophagosome is formed, which will later fuse with the lysosome to form the autolysosome. Then, the captured material is degraded by the hydrolase enzymes present in the lysosome [18–21].

The important PI3K/Akt/mTOR pathway is a signaling pathway of the autophagy process and begins with the PI3K and Akt proteins that are responsible for positively regulating the mTOR protein [22–24]. In this sense, by means of therapeutic agents, the possibility of manipulating the pathways and proteins involved in the autophagic process is a welcome strategy in the fight against cancer [25].

It is known that autophagy, when related to cancer, has a dual behavior, i.e., it can either help cancer cells not to form or help already-formed cancer cells to survive [26]. This duality has so far divided numerous opinions in the scientific community. While nowadays, it is possible to understand that the possibility of manipulating autophagy, either inducing or inhibiting it (by means of pathways, proteins, drugs, etc.), is an important reality for cancer treatments [25], after all, as it is known, cancer is divided into stages and, therefore, the manipulation of autophagy can be a great advantage [27].

On this basis, vanadium complexes are usefully reported in the literature for acting in the autophagy processes [28–35]. In this work, a vanadium complex that has proofed efficiency in inhibiting the autophagic process in pancreatic cancer cells (Fig. 1) was the object of study [31].

Understanding how the inhibition of autophagy occurs at the molecular level, i.e., what are the interactions between the molecular targets and the vanadium complex, can be perceived as a study that will provide important contributions to the field. In this sense, classical molecular dynamics (MD) simulations can assist in this type of investigation.

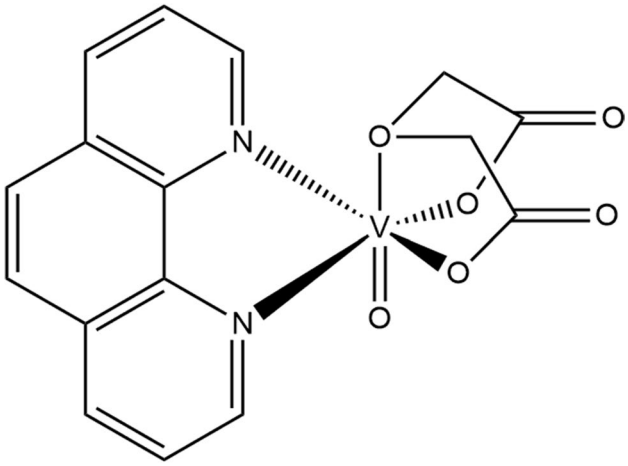

Fig. 1 Vanadium complex (VC) under study, [VO(oda)(phen)]

However, MD simulations are strongly dependent on the proper choice of force fields, and it is also known that force field parameters for inorganic compounds are scarce and often not represented by standard force fields [36–39]. Furthermore, general force fields have a small number of atomic types, making it impossible to describe a wide-ranging number of compounds [40, 41].

Regarding the parameterization of vanadium complexes, the development of specific force field parameters for this coordination environment of vanadium and specific type of complex (Fig. 1) has not yet been reported in the literature. Moreover, making use of a general force field may not favor satisfactory results leading to unrealistic structures [42]. Thus, the need to develop specific force field parameters for the vanadium complex, the target of this study, is crucial.

Based on the above considerations, the goal of this work is divided into three parts: (i) To report the development of AMBER force field parameters, specific for the complex [VO(oda)(phen)], from a minimum energy structure, obtained by quantum mechanics calculations (DFT). After that, (ii) to validate this new force field by implementing these new parameters to classical molecular dynamics simulations and comparing the post-calculation properties with experimental values [43] and the quantum reference (DFT). Finally, as mentioned previously, the manipulation of autophagy by therapeutic agents may be an excellent strategy to combat cancer [25]. Thus, the last goal is (iii) to investigate the types of interactions that occur between the vanadium complex and the protein responsible for initiating the autophagy signaling pathway (PI3K).

Computational details

QM calculations

The initial structure of the complex under study (Fig. 1) was optimized through quantum mechanics calculations with B3LYP level of theory (exchange-correlation functional, used in Density Functional Theory-DFT) and the basis set def2-TZVP for ligand and LANL2DZ ECP for vanadium. This level of theory was successfully used and validated by Kaur and collaborators in purely theoretical investigations for vanadium complexes [44, 45]. In this step, the Gaussian 09 software [46] was used.

Furthermore, using the software ORCA 4.0 [47], relativistic effects on the vanadium complex were investigated with B3LYP/def2-TZVP level of theory through relativistic method ZORA. The ZORA-def2-TZVP basis set was successfully used for the vanadium metal by Cárdenas and co-workers recently [48].

Based on the lowest energy spatial arrangement found, the calculations of the non-polarizable RESP (restrained electrostatic potential) partial atomic charges [49] and the Hessian matrix were performed with the same level of theory and software as the optimization calculation. This last calculation, based on the Seminario method [50], allowed the values of the force constants for the bonded terms to be obtained through the diagonalization of the Hessian matrix, using the Paratool plugin [51], available on the software VMD (visual molecular dynamics) [52].

To validate the developed force field, an MD simulation was performed in vacuum ($T = 300$K) using the AMBER 20 package [53], with a simulation time of 20 ns. The developed parameters were validated through structural analysis of the bond lengths and bond angles of the complex, RMSD, and bond length alternation (BLA) analysis. In addition, we investigated the symmetry of the molecule through the developed force field (FF). All results were compared with experimental values [43], quantum mechanics calculations, and values obtained by GAFF. Regarding the MD performed using GAFF, there are no parameters for metals in this force field. Therefore, for the bonded terms involving the vanadium atom, the parameters developed and validated by us in this work were used.

Development of force field parameters

In classical molecular dynamics (MD) simulations, the force acting on each of the particles in the system is obtained by the contribution of each interaction with the other particles involved. Such forces are described by the potential energy functions of the structural contributions, bond lengths, bond angles, and dihedral angles, as well as interactions between non-bonded atoms [54].

Thus, potential energy (V) is the energy that describes a given system and can be expressed, in general, as follows:

$$V_{\text{total}} = \sum_{\text{bonds}} K_b\left(b - b_0\right)^2 + \sum_{\text{angles}} K_\theta\left(\theta - \theta_0\right)^2 + \sum_{\text{dihedrals}} K_\phi[\cos\left(n\phi - \delta\right) + 1] + \sum_{\text{Coulomb}} \left[\frac{q_i q_j}{4\pi\varepsilon_0 r_{ij}}\right] + \sum_{\text{Lennard-Jones}} 4\epsilon_{ij}\left[\frac{\sigma^{12}}{r_{ij}^{12}} - \frac{\sigma^6}{r_{ij}^6}\right] \quad (1)$$

where K_b, K_θ, and K_ϕ are force constants; b and θ correspond to the bond length and bond angle, respectively; b_0 and θ_0 are the equilibrium values; n is the periodicity; ϕ is the dihedral angle; δ is the phase angle; r_{ij} is the distance between atoms i and j; ϵ is the depth of the potential well; σ is the distance at which the Lennard-Jones potential is zero; q_i and q_j are the charges of each atom; and ε_0 is the permittivity in vacuum. Equation (1) describes a typical force field, known as AMBER force field [55].

In general, the parameterization of intermolecular potentials (V_{Coulomb} and $V_{\text{Lennard-Jones}}$) is a great challenge and, in addition, obtaining these parameters in particular may result in loss of precision of intramolecular parameters. Thus, it is important to inform that in this work, the parameterization of the intramolecular potentials was carried out, i.e., the parameters referring to the potentials V_{bonds}, V_{angles}, and $V_{\text{dihedrals}}$.

The force constants presented in Eq. (1), the equilibrium values, as well as the periodicity and the phase angle values were obtained by calculating the Hessian matrix ("QM calculations" subsection). To collect the data provided by the diagonalization of the Hessian matrix, the *Paratool* plugin [51], available in VMD software [52], was used. In this step, the atomic types (atom types) were defined.

Regarding MD simulations in AMBER, it is necessary to define the atom types with only two characters. In this work, the characters used were letters and numbers (Fig. 2). In addition, for the values of the bond length (K_b) and bond angle (K_θ) constants that were equivalent (i.e., mirrored), an arithmetic average was performed to consider the symmetry of the molecule. An example of symmetric bonds is the V1-O2 and V1-O5 bonds, and an example of angles that are symmetric is the N1-V1-O2 and N2-V1-O5 angles.

Next, to obtain the Lennard-Jones potentials, σ and ϵ, it was necessary to search the literature for GAFF (general AMBER force field) data regarding these two parameters. Thus, based on the investigation conducted by Wang and collaborators [57], it was possible to collect the parameters σ and ϵ for all the vanadium complex atoms, except for the vanadium metal. The van der Waals parameters for the vanadium atom were obtained based on a study of Šebesta and

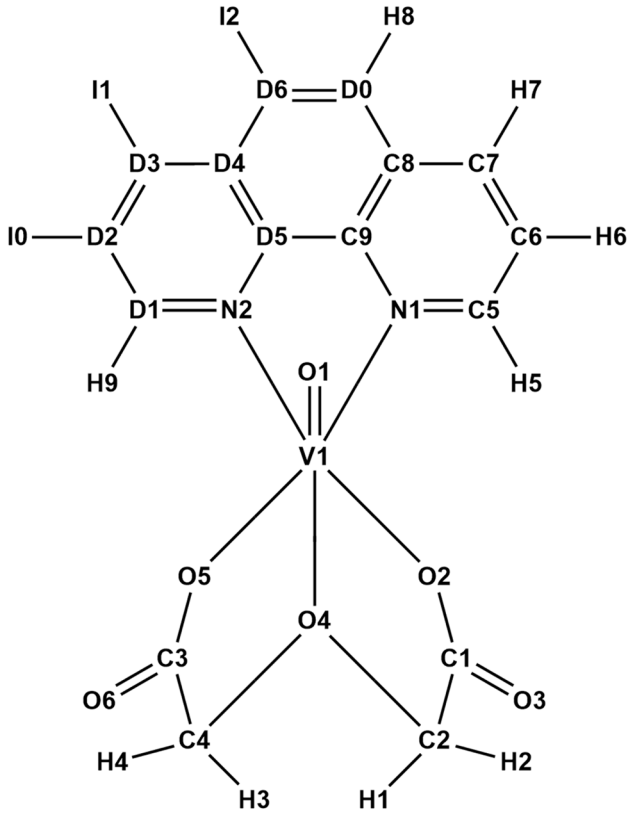

Fig. 2 Atom types assigned to the atom types (VC). Image generated using software *ChemDraw Ultra 12.0* [56]

collaborators [58], since the parameterization of GAFF [57] was done targeting organic molecules.

Finally, obtaining the Coulomb interaction parameters of the vanadium complex, q_i and q_j, was performed by calculating the non-polarizable RESP partial atomic charges ("QM calculations" subsection). For this calculation, the same functional and basis function used in the optimization calculation was adopted.

The final layout of the topology file, according to Fig. 2 and containing all the information described in this section, can be found in the Supporting Information (SI) file made available by the authors (Section S2). The values corresponding to the RESP charges are also found in the SI (Table S4).

PI3K protein treatment

The Protein Data Bank (PDB) database provides crystallographic structures of several proteins, including PI3K (code 3QJZ [59]; resolution = 2.90 Å). However, there are absent residues in the crystal of the molecule, which could lead, in a way, to inaccurate results in its analyses. Thus, we performed a treatment of the PI3K protein so that the missing residues are described within the PDB of the molecule, providing more reliable results.

To generate the protein model that contains all the original and the missing residues, the SWISS-MODEL platform [60] was used. After that, it was necessary to evaluate the model generated by the platform. Thus, we performed an alignment between the protein generated by SWISS-MODEL after completing the missing residues and the original protein (code 3QJZ [59]), using the "LovoAlign" protein structural alignment package [61]. From the aligned protein, we calculate its RMSD with relation to the original protein. The overlap between the two proteins (complete/aligned and original) is available in the Supporting Information file (Figure S1, Section S3).

Molecular docking calculations

Using the MolDock algorithm, present in the Molegro Virtual Docker (MVD) software [62], VC was docked within the human PI3K protein. The binding site considered for the docking study was the same used by Gurumoorthy and collaborators [63], where it was shown that the phenanthroline (*phen*) ligand promotes an interaction with the Arg839 residue of PI3K. Such interaction was evaluated in this study.

After further investigation to evaluate the best parameters for the best performance of docking with VC, a binding site within a restricted simulation space of 10 Å was considered. In addition, residues within a radius of 12 Å were considered flexible. At the end of the docking simulation of the complex on the protein, 100 poses were generated. Of these 100 poses (conformations and orientations of the VC), the pose that showed the lowest energy of interaction and indicated an interaction with residue Arg839 was chosen as the starting point for the next step, the molecular dynamics simulation.

Molecular dynamics simulations

The three preparation steps for Molecular Dynamics (MD) simulation, plus the last production step, were performed using PMEMD software [64], included in the AMBER 20 package [53].

As previous commented, the simulations were divided into four steps, namely: minimization, heating, equilibrium, and production. To perform the four steps, the force field "leaprc.ff14SB" was used to simulate the protein [65, 66]. On the other hand, to simulate the vanadium complex, the force field developed and validated in this work was used. Furthermore, the simulations were carried out with explicit solvation which incorporated a cubic TIP3P water box [67]. Water molecules were added within a radius of 25 Å from the protein to the edge of the simulation box. Nine counterions (Na^+) were added to neutralize the system. To

counterbalance the charges of the amino acids in the protein, the neutral pH was considered, and the program *leap* was used. All four steps were performed considering the work of Arba et al. [65] and Farrokhzadeh et al. [66].

The first step (minimization) was performed to remove the bad contacts between the atoms, and to prepare the system for the heating step. This simulation was divided into two steps, the first simulation (min1) performed with a system restriction of 500.0 kcal/mol and the second simulation (min2) performed without restriction. Both steps were performed at constant volume with 500 cycles of steepest descent and 5500 cycles of conjugate gradient methods.

In the next step, the system was heated gradually from 0 to 100 K (heat1), 100 to 200 K (heat2), and 200 to 300 K (heat3), each step being performed at 50 ps with a time step of 0.0005 ps and a constraint with a force constant of 5 kcal/mol. The system was then equilibrated at 300 K. For this third step, the simulations were divided into three parts, the first two steps (Eqs. 1 and 2) being performed both at 50 ps with a force constant of 5 and 3 kcal/mol, respectively. Finally, the third equilibration step (Eq. 3) was performed without restriction and with a time of 100 ps. In total, the heating step was performed at 150 ps and the equilibration step at 200 ps.

The MD simulation is finally performed in the production step, where a simulation time of 120 ns was considered in NPT ensemble without any restraint. All bonds involving hydrogen atoms were constrained using the SHAKE algorithm [68] with 2 fs integration time step. The particle-mesh Ewald algorithm method was used to treat long-range electrostatics interactions [69] of a periodic box with a non-bonding cutoff distance of 10.0 Å. In addition, the simulations were carried out using the Berendsen barostat and the Langevin thermostat [70] with a collision frequency of 1.0 ps^{-1}.

The analyses of the trajectories of all simulation steps were performed with the CPPTRAJ module [71] and visual molecular dynamics (VMD) software [52].

Results and discussion

Static calculations

Computational modeling of drug-target systems is commonly performed to determine the likely mechanism of action. In this context, molecular dynamics (MD) simulations play a prominent role in this type of approach, providing further information about the structural properties and thermodynamic parameters of molecular systems [72].

Nevertheless, one of the biggest challenges in performing MD simulations to investigate the behavior of ligands with their molecular targets is to use a force field that satisfactorily reproduces the properties of interest [73]. In the case of metal complexes, the difficulty increases significantly [55, 74].

In the HyperChem 7.0 software [75], it is possible to find the AMBER force field available for the vanadium complex (VC) under study. In addition, the UFF (universal force field) is also available for the target complex of this study in the software Gaussian 09. The result containing the relative errors of some bond lengths and bond angles is available in Table S1.

In general, metal atoms that occupy lower periods in the periodic table (sixth period onwards), have more pronounced relativistic effects. On the other hand, atoms that occupy the initial periods of the periodic table have a theoretical basis of study very well established by non-relativistic quantum mechanics [76]. Thus, the vanadium atom, which is located in period 4 of the periodic table, does not have such expressive relativistic effects. Even so, we performed calculations in the ORCA software [47], where the relativistic method ZORA is available, and a comparison of the previously mentioned data with calculations performed in the Gaussian 09 software was conducted [46].

Thus, Table S2 presents some values of VC bond lengths and bond angles, where three comparisons were made. The first is the comparison of the experimental values with the values obtained by the quantum calculation with B3LYP/def2-TZVP with ECP level of theory, where the role of the effective core potential (ECP) is to modify the basis function so that relativistic effects on the vanadium atom are considered.

The second comparison was made between the experimental data and the data derived from the quantum-mechanical calculation obtained by the same functional and basis set, but without ECP and with the relativistic method ZORA, which, in turn, modifies the Hamiltonian of the Schrödinger equation to consider relativistic effects. Finally, the last comparison (Table S2, fourth column) concerns the comparison between the two quantum mechanics calculations preciously mentioned, namely: B3LYP/def2-TZVP with ECP and B3LYP/def2-TZVP with ZORA.

It can be seen from Table S2 that the relative errors are low in all three comparisons. Furthermore, the low relative error originated from [ECP/ZORA] comparison shows that the level of theory used in this work to obtain the lower energy spatial arrangement of the vanadium complex is as effective as the relativistic method ZORA, thus validating the use of the B3LYP/def2-TZVP level of theory with ECP for vanadium. In other words, the lower energy geometry of the vanadium complex obtained by optimization with ZORA is appreciably equivalent to the result of optimization with ECP.

Dynamics calculations: validation of FF parameters

After the entire AMBER force field parameter development step ("Development of force field parameters" subsection), efforts were directed towards validating the performed parameterization. To this end, a molecular dynamics (MD) simulation was performed in AMBER 20 simulation package [53]. The simulation was performed in vacuum with a total time of 20 ns, with the temperature equal to 300 K and a time interval of 1 fs. In order to ensure that the system undergoing the simulation has reached equilibrium, only the last 10 ns were considered for further analysis.

In general, the analyses performed in this work to validate the developed force field, called here as "New_FF," were structural analyses with comparisons between the bond lengths and angles, obtained by different methods, namely: data obtained by X-ray crystallography [43]; DFT calculations with B3LYP functional and def2-TZVP and LANL2DZ ECP basis sets for vanadium; MD simulation with the new force field developed in this study; and finally, an MD simulation with GAFF force field, under the same conditions as the previous MD. In addition, analyses of RMSD, BLA, geometry, and symmetry of the molecule were performed. All the mentioned analyses are described in the following topic.

Analysis of structural properties

The first step to validate the parameterization performed in this work was to analyze the deviation of the spatial coordinate set of the complex in the simulation according to the coordinate set of the optimized geometry with DFT. This analysis was obtained by calculating the RMSD (root mean square deviation) [77] that provides the information of the difference between the predicted value (quantum reference) and the calculated value (MD with New_FF).

Based on the graph shown in Fig. 3, it is possible to see a very good agreement between the two overlapping geometries. Subtracting the largest RMSD value from the smallest value, it is possible to find an oscillation amplitude of approximately 0.6 Å. Furthermore, the average of the values of the last 10 ns is 0.3 Å ± 0.003 Å. From these results, it can be clearly seen that the geometry provided by the force field parameter set proposed in this work is quite similar to the geometry obtained by quantum mechanics calculation.

The fact that the MD simulation was performed in vacuum enriches the good results obtained after the RMSD calculation since the complex is totally free to oscillate, i.e., there are no other molecules restricting its motion in the surroundings. In this sense, even oscillating freely, the VC presents a low and stable conformational variation throughout the simulation.

Furthermore, as a means of comparison, we carried out an RMSD calculation between the MD coordinates with

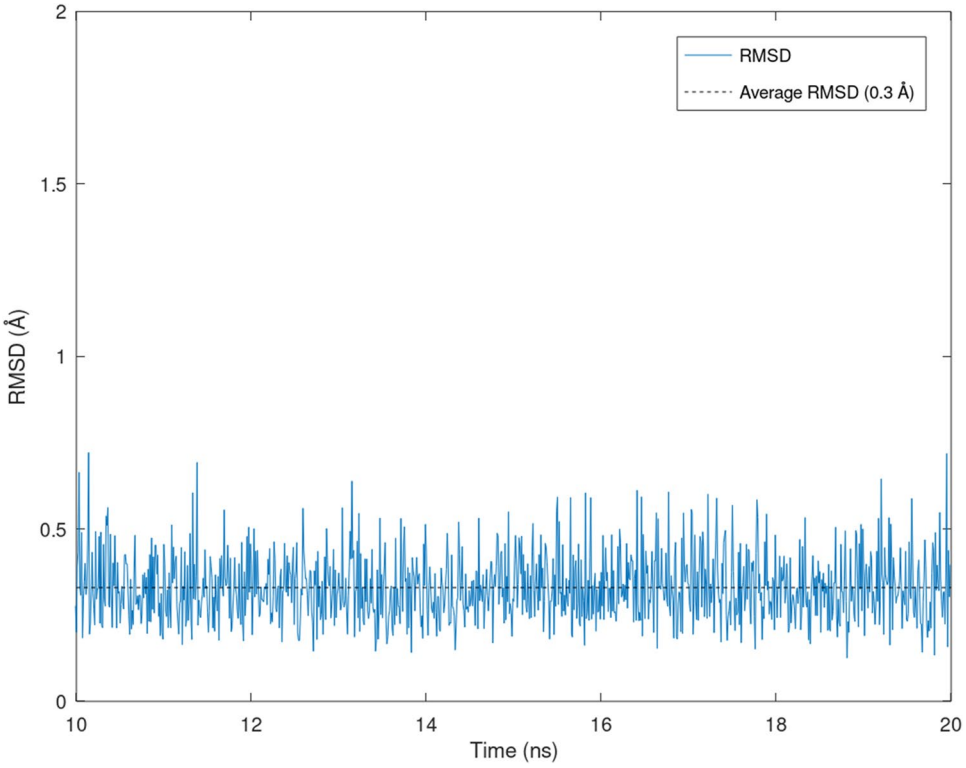

Fig. 3 RMSD values (Å) versus time (ns) of MD simulation performed in vacuum at 300 K

GAFF and the quantum reference (Figure S4). The average of the RMSD values was equal to 0.4 Å, which suggests that the performance of GAFF to describe the geometry of the VC, from the general point of view, was satisfactory. In addition, we also performed the calculation of the mean deviation for the bonds and angles of New_FF and GAFF, both with respect to the DFT values (Table S6).

In the work reported by Álvarez and collaborators [43], the geometries obtained by DFT calculations and X-ray crystallography indicated that the vanadium metal and the other atoms connected to it have a distorted octahedral geometry. On this basis, a distorted octahedral is observed in Fig. 4(a), where the spatial arrangement was obtained after a quantum mechanical (DFT) calculation. The same can be observed in Figure 4(b), where a slightly more distorted octahedral geometry was obtained from the MD simulation performed with the new set of force field parameters (New_FF). The ideal octahedral geometry cannot be found since the angles around the vanadium metal do not have 90°. In addition, as a mean of comparison, the geometry obtained with GAFF is shown in Fig. 4(c).

Moreover, it is also mentioned in the literature that the oxydiacetate ligand (oda—which corresponds to the atoms O2, O4, and O5 in Fig. 4) adopts the *fac* arrangement, and the central oxygen atom in the ligand (in our reference, oxygen O4) displays a *trans* geometry with respect to the vanadyl group (V1=O1) [43, 78]. The geometry obtained by mean of the parameterization proposed in this work also reproduces this spatial arrangement.

GAFF (general AMBER force field) is a force field often used in MD simulations, with success in many cases [57, 79–81]. Howbeit, the developers of this useful force field aimed at organic molecules, which makes it difficult to apply to metal complexes [55, 57]. Still, this work used GAFF parameters in an MD simulation in vacuum (T = 300 K) with a total simulation time of 20 ns [55]. The obtained results were confronted with experimental values [43] (Table 1).

From Table 1, the relative errors were calculated by considering Eq. (2). For example, for the O4-C2 bond and the O2-V1-O4 angle, the relative error values correspond to 2.1% and 6.5%, respectively.

$$\% = \frac{\text{calculated value} - \text{experimental value}}{\text{experimental value}} \times 100 \qquad (2)$$

The vanadium complex under study in this work is comprised of 42 bonds and 80 angles. For each bond and angle, a percentage of relative error was obtained. Thus, the arithmetic mean of the module of values was obtained.

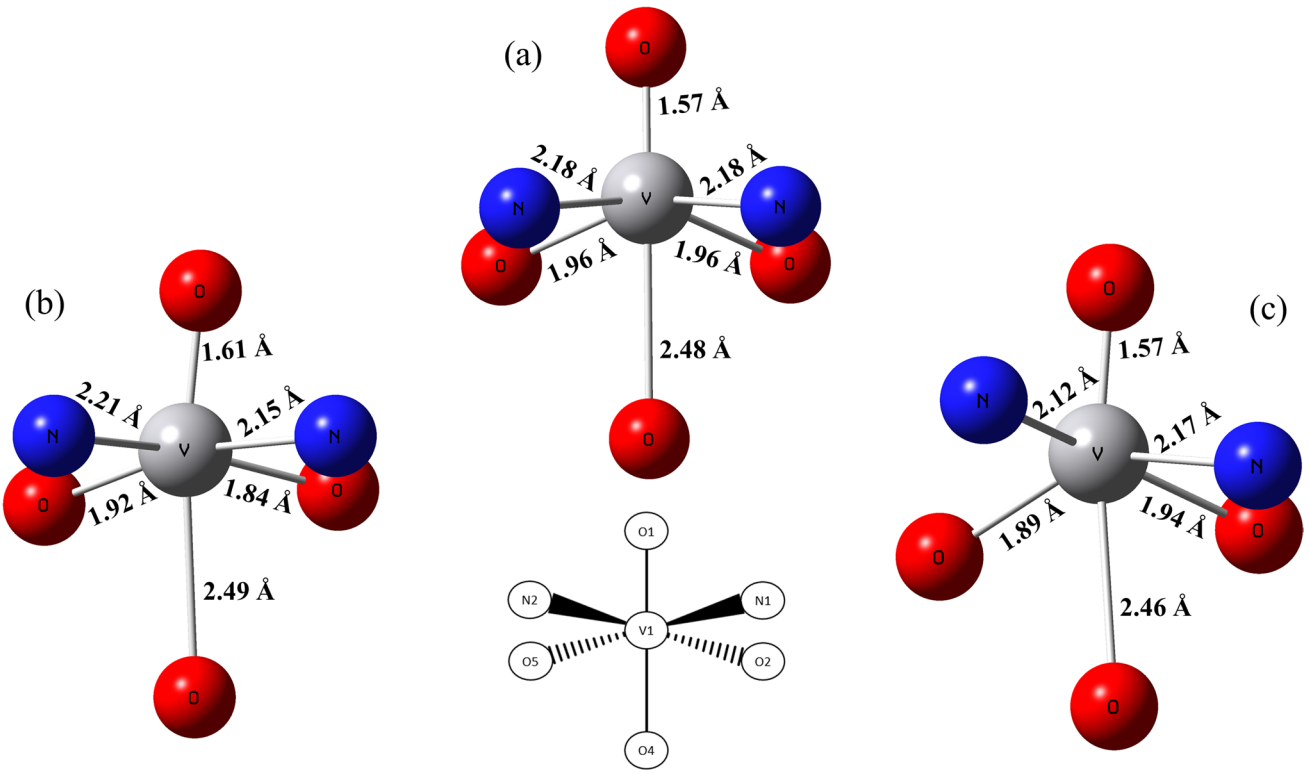

Fig. 4 Distorted octahedral geometries of the VC obtained by (**a**) DFT calculation, (**b**) MD with New_FF, and (**c**) MD with GAFF. The remaining atoms in the complex were deleted

Table 1 Bond lengths (Å) and angles (°) selected for the VC. Experimental values and average values obtained from the MD simulation with the GAFF force field

Bond lengths	Exp.	DFT	GAFF	Bond lengths	Exp.	DFT	GAFF
V1-O1	1.59	1.57	1.56	**O3-C1**	1.22	1.22	1.21
V1-O2	1.97	1.96	1.91	**O4-C2**	1.43	1.43	1.46
V1-O4	2.30	2.48	2.46	**C1-C2**	1.51	1.53	1.51
V1-N1	2.11	2.18	2.18	**O5-C3**	1.28	1.30	1.33
O2-C1	1.28	1.30	1.33	**N1-C5**	1.32	1.32	1.39
Angles	**Exp.**	**DFT**	**GAFF**	**Angles**	**Exp.**	**DFT**	**GAFF**
V1-O4-C2	108.55	107.49	102.91	**O2-V1-O4**	76.02	72.85	71.10
V1-N1-C5	127.87	126.03	127.89	**O2-V1-O5**	90.93	98.65	105.45
V1-O2-C1	123.36	128.63	129.27	**O2-V1-N1**	90.78	87.36	82.26
O1-V1-O2	101.32	105.02	107.66	**O2-C1-O3**	124.34	125.83	121.70
O1-V1-O4	176.10	176.53	165.36	**C2-O4-C4**	114.77	116.68	114.82
O1-V1-N1	101.90	99.22	94.46	**N1-C5-C6**	122.08	122.01	119.28

About 80.9% of the VC bond values, obtained from the MD simulation with the GAFF force field, varied in a relative error range of 0 to 11%. More precisely, the mean relative error of the comparison between the experimental and GAFF values was exactly 5.7%, with an average standard deviation of 0.001%.

The analysis of the bond angles was conducted in an analogous way. The average variation of the relative error of the comparison between the experimental values and the values obtained by GAFF was equal to 2.7%. In other words, the relative error ranged around almost 3%, with an average standard deviation of 0.128%. Furthermore, it can be concluded that 81.2% (which corresponds to 65 angles out of 80) ranged between 0 and 4%.

The MD simulation with the implemented GAFF force field allowed the confirmation that GAFF is not a suitable force field to describe the vanadium complex under investigation. Indeed, its purpose is to describe organic molecules; however, the VC has two organic ligands, which makes the investigation of its applicability in our system valid.

It is important to highlight that GAFF is an excellent force field; however, it is usually applied to simulate organic molecules. In this sense, for the special case of [VO(oda)(phen)], the use of a specific force field to describe this metallic complex, such as New_FF, is an advantage compared to general AMBER force field.

The proper choice of force field to use in molecular dynamics simulations is a crucial step for successful calculations and results. As mentioned previously, GAFF force field is not a suitable choice to describe the VC. Moreover, automatic force fields and those available in software Hyperchem 7.0 and Gaussian (AMBER and UFF, respectively) are not efficient to describe the molecule under study in this work. It is clear then that force fields that do not describe the system satisfactorily should be avoided.

Taking this into consideration, it is evident the need to develop a specific force field for the complex [VO(oda)(phen)] is the focus of this work. After our efforts were directed towards the parameterization of the complex, validation was performed through an MD simulation in vacuum with the new implemented force field (New_FF). Table 2 gathers some values of bond lengths and bond angles obtained from three methods, namely: X-ray crystallography (Exp.) [43]; quantum mechanical (DFT) calculations; and MD simulation with the new force field (New_FF).

Analogously to the analyses performed in the comparison between the experimental values and the MD values with the GAFF force field, the analyses of the three comparisons of the data in Table 2 were made. The comparisons conducted were the experimental values with the New_FF values (Exp/MD); values from the quantum reference (DFT) with the New_FF values (QM/MD); and finally, the comparison between the experimental values and the DFT values (Exp/QM).

Regarding the 42 VC bonds, we could conclude that 80.9% of the values of the relative errors of the Exp/MD comparison ranged between 0 and 10%. Although this seems like a wide range, the average of the values is only 4.8%, i.e., most of the relative errors oscillate around this value. In addition, the mean standard deviation was 0.001%.

The average relative error of the QM/MD comparison was 0.6%, showing an excellent agreement between the MD simulation with New_FF and the quantum reference calculation (DFT). The variation of the latter comparison was between 0 and 2% for all bonds in the VC, where precisely 20 bonds had average relative error of 0%, 18 bonds with 1%, and 4 bonds with 2%, totalizing the 42 bonds present in the molecule.

It is worth mentioning that the calculation of the relative error for the QM/MD comparison considered the value of the quantum reference as the truest value. Thus, in Eq. (2), instead of the experimental value, the value obtained

Table 2 Bond lengths (Å) and angles (°) selected for the VC. Experimental values, quantum reference values, and average values obtained from the MD simulation with New_FF

Bond lengths	Exp.	DFT	New_FF	Bond lengths	Exp.	DFT	New_FF
V1-O1	1.59	1.57	1.56	**O3-C1**	1.22	1.22	1.21
V1-O2	1.97	1.96	1.91	**O4-C2**	1.43	1.43	1.44
V1-O4	2.30	2.48	2.48	**C1-C2**	1.51	1.53	1.53
V1-N1	2.11	2.18	2.19	**O5-C3**	1.28	1.30	1.29
O2-C1	1.28	1.30	1.29	**N1-C5**	1.32	1.32	1.34
Angles	**Exp.**	**DFT**	**New_FF**	**Angles**	**Exp.**	**DFT**	**New_FF**
V1-O4-C2	108.55	107.49	101.86	**O2-V1-O4**	76.02	72.85	74.06
V1-N1-C5	127.87	126.03	129.23	**O2-V1-O5**	90.93	98.65	101.45
V1-O2-C1	123.36	128.63	127.10	**O2-V1-N1**	90.78	87.36	84.57
O1-V1-O2	101.32	105.02	106.58	**O2-C1-O3**	124.34	125.83	123.55
O1-V1-O4	176.10	176.53	172.14	**C2-O4-C4**	114.77	116.68	117.77
O1-V1-N1	101.90	99.22	94.77	**N1-C5-C6**	122.08	122.01	121.96

by the quantum mechanics calculation (DFT) was considered. The relative errors of the other comparisons (Exp/MD and Exp/QM) were obtained according to Eq. (2).

The comparison between the experimental data and the quantum reference (Exp/QM) values was performed to investigate whether the choice of the level of theory for the DFT calculations was a good choice. The range of variation for 34 bonds (representing 80.9% of the total bonds) was between 0 and 10%; however, the average of the values is only between 4.4%.

It is worth noting that the results obtained by comparing the New_FF with the experimental values (Exp/MD) showed great similarity with the comparison of the DFT values and the experimental ones (Exp/QM). In other words, our proposed new force field had errors in the same range as the errors that the quantum structure presented. Moreover, this is explicit by looking at the average relative error of the QM/MD comparison, where the relative error values merely ranged around 0.6%.

The same analyses were performed for the set of 80 angles of the [VO(oda)(phen)] complex. Results of the first comparison (Exp/MD) provide a range of relative errors from 0 to 3% for 81.2% of the total angles of the molecule. The average relative errors were 2.0% and the mean standard deviation was 0.153%.

The comparison of the results between the quantum reference values and the New_FF values (QM/MD) provided an average of a mere 1.4% and range of variation for 78.7% of the bonds (63 angles) from 0 to 2%. The Exp/QM comparison, on the other hand, indicates a range between 0 and 2% for 66 angles (82.5%), with an average error of 1.3%.

Remarkably, low values are shown in the comparisons of the angles of the MD using the New_FF with the experimental and quantum reference values. Strictly speaking, the force field developed by us shows excellent agreements, with the average relative errors of the bond angles for Exp/MD and QM/MD comparisons being 2.0% and 1.4%, respectively.

In references [78, 82], the authors synthesized a few vanadium complexes, among them, the complexes [V(O)(oda)(H2O)2] **1**, [V(O)(oda)(N-N)].H2O (N-N = bipy, **4**; phen, **5**). Complex **1** provides experimental values of some structural parameters and parameters of the molecule with *fac* arrangement, obtained after a DFT calculation (B3LYP/LANL2DZ level of theory). Moreover, after X-ray analysis, the authors showed that system **4** obtained two independent molecules and that such molecules show little difference between each other.

Although complex **5** is identical to the complex under study in this work, the authors reported that the crystal quality was poor, making it impossible to represent the complex in detail. Even so, based on comparisons with the other complexes, especially complex **4**, the authors were able to extract important information about complex **5**. Thus, the information obtained from the analysis of the three complexes mentioned above were useful for our work.

Based on the parameters presented in Table 2, especially regarding the Exp/MD comparison, some bond lengths and bond angles showed relative errors greater than 3%. Therefore, these parameters are discussed below.

The V1-O4 bond (2.48 Å), obtained by New_FF, was overestimated compared to its respective experimental value (2.30 Å), providing a relative error of 8.0%. However, in [78] this bond is also overestimated. This occurs both for complex **1** ([V(O)(oda)(H_2O)$_2$]) in its *fac* arrangement (2.44 Å) and for complex **4** ([V(O)(oda)(bpy)], which has great similarity with the system under study in this work ([VO(oda)(phen)]) in the two molecules found, with values of 2.32 Å and 2.33 Å, respectively.

Additionally, when comparing the obtained value of the V1-O4 bond with the New_FF (2.48 Å) and the quantum reference (2.48 Å), a relative error of 0.04% is found. As commented earlier, the comparison between the experimental and DFT (Exp/QM) data provided excellent agreement, which allows us to validate the obtained value of the V1-O4

bond (2.48 Å) based on the value obtained by the quantum reference.

The V1-O2 bond (1.91 Å) was underestimated by New_FF compared to the experimental value (1.97 Å). However, in [78], the *fac* arrangement of complex **1**, similar to the *fac* arrangement of the VC under study in this work, shows the value for the V1-O2 bond of 1.92 Å, which provides a small relative error (0.5%) compared to the value given by New_FF.

Finally, the V1-N1 bond showed an experimental value of 2.11 Å, while the MD simulation with the new force field provided a higher value of 2.19 Å. This led to a relative error of almost 4% (3.8%). In spite of that, looking at the bias of the QM/MD comparison, a relative error of 0.46% was found, since the quantum reference value for this bond was 2.18 Å. This understanding is acceptable, mainly because the validation of New_FF in this study is done based on two references, experimental values and values coming from quantum mechanics (DFT) calculations.

From the point of view of the bond angle analysis, it is already expected that the angle values will oscillate more compared to the bond length values. This is expected because the angle force constants (K_θ) are smaller than the bond force constants (K_b) (see Section S2). Thus, the angular deformations are larger than the bond stretches. For this reason, angles in Table 2 with relative errors above 5% are discussed below.

Regarding the O1-V1-O2 bond angle, the new force field showed a higher value (106.58°) compared to the respective experimental value (101.32°). This angle also shows overestimated values in [78], with the complex [V(O)(oda)$(H_2O)_2$] showing *fac* arrangement and experimental values of 106.95° and 108.30°, respectively. Furthermore, the relative error of the QM/MD comparison for this angle was 1.5%, where the quantum reference value was 105.02°.

For the angle O2-V1-N1, the MD simulation with the new force field provided a value of 84.57°. The experimental value, on the other hand, was exactly 90.78°. Although suggesting a somewhat high difference, the quantum reference value (87.36°) was close to the New_FF value, yielding a relative error of 3.2%.

The experimental value of the O2-V1-O5 bond angle, obtained by X-ray crystallography, was 90.93°, a bit far from the value provided by New_FF (101.45°). However, this value can be validated by comparing with the value (101.60°) provided in [78] of its analogous complex (**1**), where the *fac* arrangement was found (spatial arrangement equivalent to that of VC). Moreover, in the comparison with the quantum reference (QM/MD), we found a relative error of only 2.8%.

The O1-V1-N1 bond angle has an experimental value of 101.90°. The force field developed in this work provided an underestimated value of 94.77° for this angle, but values of the similar complex (**4**) [V(O)(oda)(bipy)] [78] were also underestimated when compared to the experimental data. The DFT (quantum reference) value was 99.22°, giving a relative error of 4.5%. We consider this error acceptable, since angular deformations are more pronounced than bond stretches, as commented earlier.

Finally, the value of the V1-O4-C2 angle obtained by New_FF, DFT, and the experimental value were 101.86°, 107.49°, and 108.55°, respectively. The works cited do not comment on this angle; however, an individual look at this angle does not portray the efficiency of the newly developed force field. Thus, the values of all the bond angles taken together provide the understanding that New_FF can satisfactorily describe the set of bond angles of the vanadium complex [VO(oda)(phen)], the target system of this work.

By looking at Fig. 2, it can be seen that there is a symmetry in the vanadium complex, where, for example, the V1-O2 and V1-O5 bonds are equivalent of each other, likewise the V1-N1-C9 and V1-N2-D5 angles are equivalent of each other. Some selected bond lengths and angles are gathered in Table S3, where a perfect symmetry between the experimental values is remarkable.

Regarding the values found after the MD simulation with New_FF, excellent results are found, with differences only in the last decimal places. It is suggestive to remember that in each value of length and bond angle from the New_FF has an associated standard deviation. Thus, it is understood that the new force field proposed in this work was able to efficiently reproduce the proposed symmetry in the vanadium complex.

In the system under study in this work, one of the vanadium atom ligands is phenanthroline, *phen*. This ligand is a bidentate heterocyclic organic compound, where three rings are connected to each other with alternating single and double bonds (Fig. 2). Thus, it was included in the Supporting Information file an analysis of the bond length alternation (BLA), Figure S5.

Biomolecular study: (vanadium complex)–protein interactions

A treatment with the PI3K protein was performed so that the missing residues were recovered. This procedure was performed using the SWISS-MODEL platform [60], as well as an alignment between the original protein and the one obtained through the "LovoAlign" program [61].

From this treatment, it was possible to recover 150 residues that were absent. The new number of residues, as well as those that were rescued, is available in the Supporting Information file, Table S5 (Section S3). In this work, we used the new numbering to identify the residues, since, from the molecular dynamic simulation, we found interactions

between the VC and residues that were not described in the original protein file. However, the reader will be able to make the equivalence with the original protein file by observing Table S5 in Section S3.

Even with the large number of new residues in the protein file, a RMSD of only 0.84 Å was obtained between the original protein and the complete, aligned protein. Supported by this value, as well as the good overlap observed between the two proteins (see Figure S1, in Section S3), it was possible to use the improved protein and perform more reliable docking and molecular dynamics simulations between the vanadium complex and PI3K biomolecule.

Docking

Molecular docking simulations are well known for providing valuable information about the mechanism of action of a given ligand within a biomolecule, as well as providing remarkable relevance in the process of new drug discovery [83]. One important information that can be extracted from a docking calculation is the hydrogen bonds that a ligand performs with specific residues of the protein. The Molegro Virtual Docker (MVD) software [62] can be useful in evaluating such interactions.

In this context, as can be seen in Fig. 5(b), four hydrogen bonds were indicated after docking simulation. The vanadium complex (VC) forms hydrogen bonds with the Arginine 697 (Arg697) and Lysine 526 (Lys526) residues of PI3K.

The pose (conformation and orientation of the VC) shown in Fig. 5(a) was chosen based on two criteria. The first criterion was guided by the choice of conformation and orientation of the complex within the protein. As mentioned earlier, it is known that the phenanthroline (phen) ligand, present in VC (Fig. 1), exhibits interactions with the amino group of Arginine 839 [63] (Arginine 697 in our nomenclature). This information is reaffirmed by our docking study. By looking at Fig. 5(b), it is possible to see that the nitrogen (N1–Fig. 2) of phenanthroline forms a hydrogen bond with the H of the aminogroup of the Arg697 residue (2.27 Å).

In addition, a second criterion was assigned from the energetic information that the interaction of the VC with the protein provides. The most favorable conformation and orientation (i.e., lower energy, therefore more stable) indicates better accommodation of the ligand within the binding site of the protein.

The pose observed in Fig. 5(a) shows an intermolecular interaction energy of −119.79 kcal/mol. Therefore, based on the reported energy value, we can suggest that the vanadium complex does indeed interact with this PI3K binding site with favorable energy and conformation. Thus, the configuration obtained after the docking calculation is useful to serve as a starting point for other simulations, such as molecular dynamics simulations.

In general, it is important to note that, although docking studies provide important information at the molecular level of ligand-protein interactions, this type of study is not performed over time. In other words, investigations of this type provide information about a certain instant of time, which suggests to us that further investigations, over time, would be necessary.

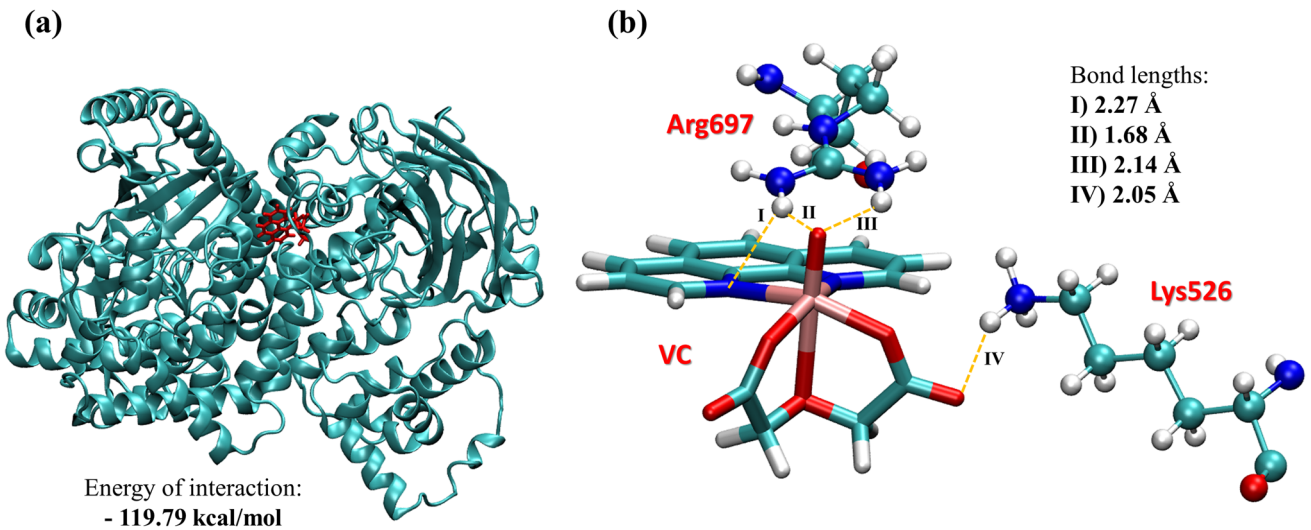

Fig. 5 (**a**) Most favorable pose of the vanadium complex within the PI3K binding site and its energy of interaction. Complex in red. (**b**) Hydrogen bonds (in orange) formed between VC and residues Arg697 and Lys526. The bond lengths are pointed out

Molecular dynamics

RMSD analysis

As previously stated, the best pose found in the molecular docking study was used to perform the MD step with explicit solvent. The RMSD calculation was performed considering the docking structure as coordinate reference. In this way, it was possible to observe the behavior of the protein and the complex over the course of 120 ns simulation (Fig. 6).

The RMSD showed a low standard deviation value indicated throughout the simulation, only 0.74 Å, i.e., the complex had an oscillation smaller than 1 Å. In addition, the MD simulation revealed that the vanadium complex has two conformations, which can oscillate during the simulation time, being conformation I with values below 1 Å (highlighted in orange in Fig. 6) and conformation II with values above 1 Å (highlighted in green in Fig. 6).

In Figure S2, we present the two conformations obtained after the MD simulation. As can be seen, the difference occurs with the oxydiacetate ligand (oda), where in conformation I, the O1 atom is away from the viewer and the O4 atom is towards the viewer. The opposite occurs with conformation II. The spatial arrangement of the other atoms of the (oda) ligand can be seen in Figure S2.

Regarding the protein, the average oscillation was 3.30 Å. Furthermore, the standard deviation value was only 0.42 Å. Since this is a simulation where the effect of the solvent and the thermal effect are taken into account [84], we considered the mean value of the oscillation to be low, especially the observed standard deviation value.

Hydrogen bonds analysis

Using the VMD (visual molecular dynamics) software [52], it was possible to identify hydrogen bonds (H-Bonds) between the vanadium complex and the PI3K protein during the MD simulation trajectory (120 ns). H-Bonds with cutoff radius of 3.5 Å and cutoff angle of 30° were considered.

The interaction reported in the docking study between residue Arg697 and the phenanthroline ligand (Arg697@N1), mentioned by Gurumoorthy et al. [63], was not reported in our MD simulation. In our best knowledge, we could not compare our MD results with the work [63] since they did not perform this simulation, only docking.

On the other hand, we found interactions between Arginine 697 and the O1 of the vanadium complex. Therefore, the two H-Bonds between O1 and the Arg697 residue found after the docking simulation (see Fig. 5(b)), were also found in our MD simulation, as can be seen in Fig. 7(a).

It is also noteworthy that in the docking study ("Docking" subsection), in addition to indicating an interaction with the amino acid Arg697, we have mentioned a new VC interaction with the residue Lys526 (see Fig. 5(b)). We found this bond (Lys526@O6(I)) in the MD simulation as well, as it can be seen in Fig. 7(b).

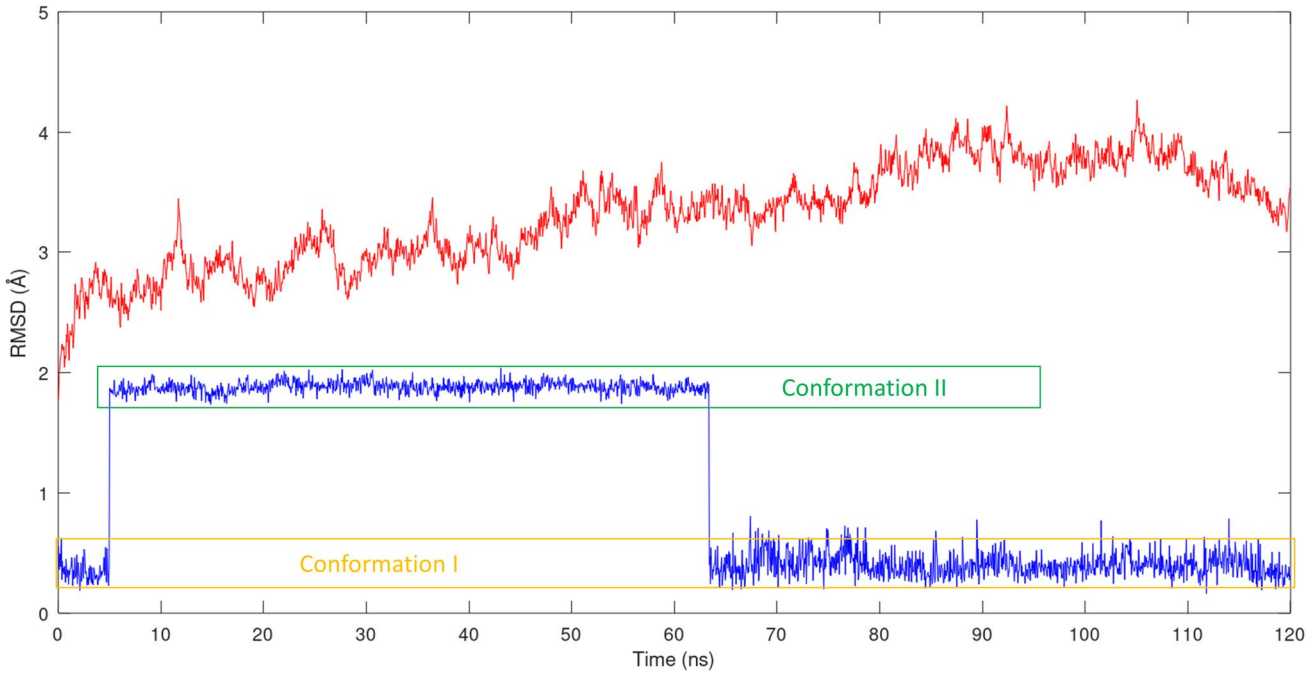

Fig. 6 RMSD analysis of the evolution of VC (in blue) and PI3K (in red) during 120 ns of simulation. The docking structure was used as coordinate reference for the calculation.

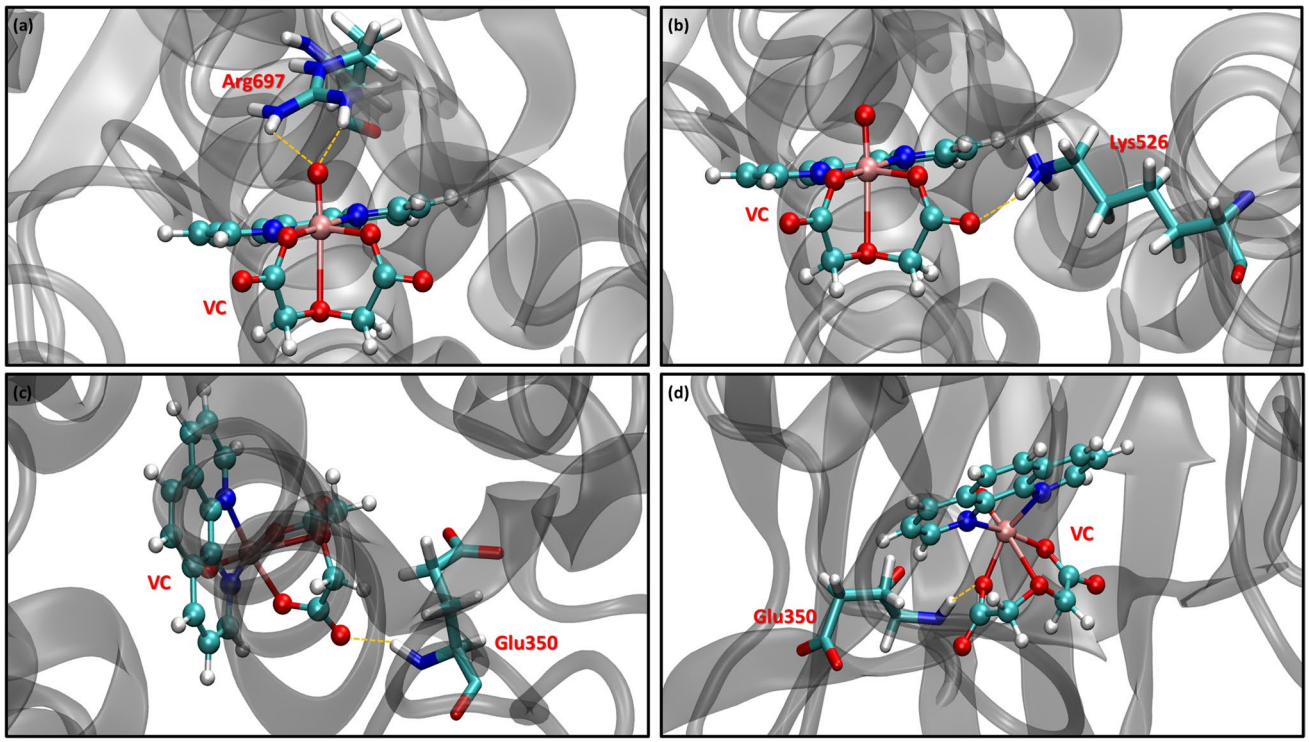

Fig. 7 (**a**) Two H-Bonds Arg697@O1(I). (**b**) H-Bond Lys526@O6(I). (**c**) H-Bond Glu350@O6(I). (**d**) H-Bond Glu350@O2(II). Hydrogen bonds in orange

In addition to the abovementioned residues, another residue stands out for having significant frequencies of occurrences throughout MD simulation, Glu350. Regarding conformations I and II, this residue presented a frequency of 71.29% and 57.88%, respectively. Thus, we tracked the main atoms of VC that performed interactions with this residue.

Two intermolecular interactions between VC and Glu350 can be highlighted, the first interaction being with the O6 atom (Glu350@O6(I)) and the second with the O2 atom (Glu350@O2(II)), Fig. 7 (c) and (d), respectively. Other VC atoms also form H-Bonds with the amino acid Glu350 (as O1, O3, and O5); however, the predominant occurrence during the 120 ns is of the Glu350@O6(I) and Glu350@O2(II) interactions.

Through the analysis of Fig. 7, it becomes interesting to observe that the vanadium complex always acts as an electron acceptor with respect to the PI3K protein residues. All pointed residues donate electrons from the N–H bond. In line with this, in all cases, the vanadium complex accepts electrons through the high electron affinity of the oxygen atoms in the complex.

The main hydrogen bonds, i.e., those involved in docking and MD simulations, as well as those that appeared more frequently, were described in the previous lines. However, we did find other H-Bonds. Although less frequent than those reported in Fig. 7(c) and (d), H-Bonds such as those shown in Figure S3 were detected after the MD simulation, namely: Asn829@O3(I) and Gln899@O1(II). On the other hand, H-Bonds with a minimum frequency of occurrence were not presented.

An important observation to make is the fact that H-Bonds such as Glu350@O6(I) (Fig. 7(c)), Glu350@O2(II) (Fig. 7(d)), Asn829@O3(I) (Figure S3(a)), and Gln899@O1(II) (Figure S3(b)), were found in residues that were not present in the original PI3K protein file. This reinforces the importance of the treatment performed with PI3K ("PI3K protein treatment" subsection), where we complete and align the protein before submitting it to the biomolecular study. The interactions cited would never have been observed if this previous treatment had not been carried out.

The combination of docking and MD simulations provides an elegant study of the interactions between a ligand and a molecular target. After the molecular docking calculation, it is suggestive to complement it with an MD simulation, due to the consideration of the effect of the solvent, as well as the thermal effect, allowing energy barriers to be overcome and thus new interactions to be pointed out [84].

In general, the atoms predominantly involved in hydrogen bonds were O1, O2, O3, O5, and O6. In addition, in a nutshell, we can also mention that the residue most involved in H-Bonds, in both conformations, was glutamic acid 350 (Glu350).

We suggest that the most stable conformation is conformation I. This conformation has *x*, *y* and *z* coordinates very close to the spatial coordinates of the docking structure (see Fig. 6, where the RMSD was calculated with reference to the docking structure). Conformation II has an RMSD close to 2 Å, i.e., it moves further away from the reference. From our findings, conformation I is closer to quantum reference, and more importantly, the spatial arrangement observed in I is consistent with the crystallographic structure of the VC. Furthermore, the difference between conformation I and II was equal to 42.58 kcal/mol. Due conformation I being more favorable, it is, possibly, the biologically active one.

Now, an important question is, what causes the VC to remain in conformation I? At the beginning of the simulation, where the complex is in conformation I, it is observed that the residue Arg565 appears with high frequency (138%), while after the change to conformation II, this percentage decreased sharply (1.20%). The same scenario is observed with residues Lys526 (90%(I)–2.14%(II)), Ser564 (71%(I)–0%(II)), Arg697 (41%(I)–2.48%(II)). Thus, our data point out that these residues are responsible for sustaining conformation I in the first moments of the simulation.

However, an important point is that, when returning from conformation II to conformation I (after 60 ns), the interactions with these residues are not restored. It is possible to attribute this to the fact that after more than half of the simulation had taken place (52.8%), the ligand moved slightly within the binding site. This can be confirmed by the fact that the interactions previously observed in conformation I (at the beginning of the simulation), are not the same observed in the second moment (i.e., after 60 ns of simulation). In this second moment of conformation I, the most accentuated interaction happened with residue Asn829. Thus, for this moment, our findings put in evidence that the amino acid residue Asparagine 829 is responsible for sustaining the VC in conformation I.

Analysis of autophagy inhibition through PI3K activation

The autophagy signaling pathway, PI3K/Akt/mTOR, is initiated by the PI3K and Akt proteins, which are responsible for positively regulating the mTOR protein. The mTOR negatively regulates the ULK1 protein, which in turn inhibits the entire autophagy process [85]. This can be understood more clearly through Scheme 1 presented below.

The vanadium complex (Fig. 1) studied in this work is known for its ability to inhibit autophagy in pancreatic cancer cells [31]. Using this information and knowing the role of each protein in the autophagy signaling pathway (Scheme 1), it is possible to understand the action of VC against each of the proteins in the pathway.

For instance, the role of VC in interactions with the PI3K protein would be to activate this molecular target. By activating such protein, Akt will be activated, which in turn will activate mTOR, and the whole cascade will follow to inhibit autophagy. A different scenario would be seen in VC's actions with the ULK1 protein, where, in this case, the complex would have the role of deactivating the protein for autophagy inhibition to occur.

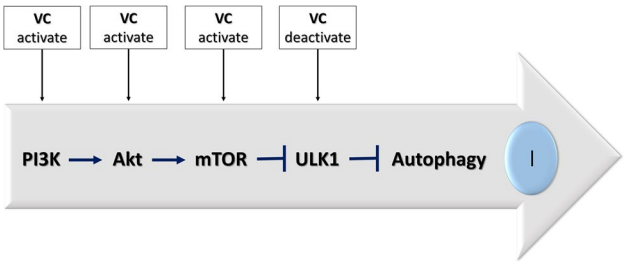

Scheme 1 Negative regulatory pathway of autophagy and performance of VC in interactions with each protein of the signaling pathway

In this work, we sought to investigate the action of VC with the protein responsible for initiating the autophagy signaling process (PI3K). VC is able to inhibit autophagy, so its action with respect to the PI3K protein is to activate this molecular target. Thus, our study could contribute to understanding how this activation occurs at the molecular level. For this purpose, the study of which hydrogen bonds occur during the MD simulation (previous topic), could be useful.

It was previously mentioned that the amino acids Arg565, Lys526, Ser564, Arg697, and Asn829 were responsible for sustaining the conformation I (more stable). Furthermore, the oxygen atoms of VC, with the exception of O4, were the most frequent in the intermolecular interactions. Based on this information, it is possible to suggest that the activation of PI3K occurs through these residues with the oxygens O1, O2, O3, O5, and O6.

Thus, to explore the manipulation of autophagy (due to its importance against cancer [25]), we can suggest that the opposite scenario, for instance, the deactivation of PI3K and thus induction of autophagy, can be achieved through modifications in the VC structure. However, it is important to emphasize that further studies are necessary for a better understanding of the manipulation of autophagy by therapeutic agents such as vanadium complexes. Thus, in the near future, efforts will be directed to a complete investigation of the autophagy signaling pathway.

Conclusions

In this work, we proposed three steps, the first being the development of the parameters; the second, validation of the new force field; and finally, a biomolecular study on protein-ligand interactions. The first part consisted of obtaining

each parameter present in the potential energy equation that describes the AMBER force field. The second part focused on the validation of the developed parameter set. For this purpose, an MD simulation was performed in vacuum (300 K) with the new parameters implemented.

All our findings confirm the excellent performance of the AMBER force field parameters developed specifically for the vanadium complex under investigation in this work. From the structural analyses, it can be considered that New_FF has been properly validated through comparisons with the experimental and quantum reference. Moreover, as comparative means, the difference in efficiency (when it comes to VC) between our force field and the widely used GAFF force field is clear.

In the last step of the work, we performed a study at the molecular level of the interactions between the vanadium complex and the PI3K biomolecule, a protein that is responsible for initiating the signaling of the autophagy process. This step consisted of two important types of molecular modeling simulations: docking simulations and classical molecular dynamics.

By performing the molecular docking simulation, the interaction between VC and the target protein was investigated. The interaction energy suggests that the VC interacts with PI3K at the considered binding site in a favorable and stable manner. Furthermore, our simulation demonstrated that the N1 of the phenanthroline ligand of VC forms a hydrogen bond with the amino group of the Arg839 (in our nomenclature: Arg697) residue of PI3K, as reported by the literature [63]. Therefore, the most stable conformation and orientation from the docking simulation was used as the starting point for the MD step.

The MD simulation provided an in-depth understanding over time of the VC behavior within PI3K, with a total simulation time of 120 ns. Through RMSD analysis, it can be observed that the vanadium complex has two conformations (I and II). In addition, a standard deviation of 0.74 Å and 0.42 Å was found for the VC and PI3K, respectively. After the execution of MD, new H-Bonds were pointed out, occurring predominantly with oxygen atoms of VC (O1, O2, O3, O5, and O6).

In order to contribute to the understanding of the mechanism of action of autophagy, we suggest that the H-Bonds between the PI3K protein and VC prevalent in the MD simulation are responsible for activating the protein, so that inhibition of autophagy occurs. Furthermore, we suggest that modifications in the VC structure, such as new bonds on oxygen atoms, would provide the opposite scenario, such as deactivation of PI3K as well as induction of autophagy. Future investigations of the autophagy signaling pathway may occur to complement the present work.

In general terms, this work fills the gap left by the absence of force field parameters for the vanadium complex [VO(oda)(phen)], which has great potential for applications in autophagy and, consequently, in anticancer treatments.

Thus, the authors acknowledge that this study contributes both to the theoretical perspective of developing force field parameters for metal complexes, and to the perspective of the biological applications, providing insights about the interactions between VC and PI3K, allowing the contribution to the elucidation of the complex process of autophagy. If appropriate force field methods are used for large systems, in which ab initio calculations are highly computational-demanding, great advances can, in principle, be performed in designing proposing new vanadium complexes that are able, this time around, to induce autophagy. Moreover, the theoretical investigation developed here may serve as a starting point for other important work.

Supplementary Information The online version contains supplementary material available at https://doi.org/10.1007/s00894-023-05530-7.

Acknowledgements The authors thank the Brazilian agencies CNPq, FAPEMIG, and CAPES for the financial support.

Data availability Along with the manuscript, the authors provide the Supporting Information file that was developed to assist in the results and discussion of the paper. In addition, we are available to send any files, if requested.

Author contribution Taináh Martins Resende Santos developed the project. Taináh Martins Resende Santos, Teodorico de Castro Ramalho, and Elaine Fontes Ferreira da Cunha analyzed the data. Taináh Martins Resende Santos, Camila Assis Tavares, and Teodorico de Castro Ramalho wrote the paper. Teodorico de Castro Ramalho conceived the overarching project. Ander Francisco Pereira helped with the entire methodology.

Funding This work was carried out with the financial support of the Conselho Nacional de Desenvolvimento Científico e Tecnológico (CNPq, 307837/2014-9) and the Fundação de Amparo à Pesquisa do Estado de Minas Gerais (FAPEMIG, PPM-00831-15), and CAPES.

Declarations

Ethics approval and consent to participate Not applicable.

Consent for publication All authors fully agree with the content of this work and are aware of the publication.

Competing interests The authors declare no competing interests.

References

1. Pham Q et al (2020) Artificial intelligence (AI) and big data for coronavirus (COVID-19) pandemic: a survey on the state-of-the-arts. Ieee Access 4:1–19
2. Sung H et al (2021) Global cancer statistics 2020: GLOBOCAN estimates of incidence and mortality worldwide for 36 cancers in 185 countries. CA Cancer J Clin 71(3):209–249
3. Shah UA (2020) Cancer and coronavirus disease 2019 (COVID-19)—facing the "C words". JAMA Oncol 6(9):1330–1331

4. Golčić M et al (2022) Could fecal microbial transplantation offer a new potential in the treatment of metastatic pancreatic ductal adenocarcinoma? Med Hypotheses 161:110801
5. Gasic U et al (2020) Polyphenols as possible agents for pancreatic diseases. Antioxidants 9(6):547
6. Cheng X, Zhao G, Zhao Y (2018) Combination immunotherapy approaches for pancreatic cancer treatment. Can J Gastroenterol Hepatol 2018
7. Hosein AN, Brekken RA, Maitra A (2020) Pancreatic cancer stroma: an update on therapeutic targeting strategies. Nat Rev Gastroenterol Hepatol 17(8):487–505
8. Jin J, Teng C, Li T (2018) Combination therapy versus gemcitabine monotherapy in the treatment of elderly pancreatic cancer: a meta-analysis of randomized controlled trials. Drug Des Devel Ther 12:475
9. Petruczynik A et al (2019) Comparison of anticancer activity and HPLC-DAD determination of selected isoquinoline alkaloids from Thalictrum foetidum, Berberis sp. and Chelidonium majus extracts. Molecules 24(19):3417
10. Haque A, Brazeau D, Amin A (2021) Perspectives on natural compounds in chemoprevention and treatment of cancer: an update with new promising compounds. Eur J Cancer 149:165–183
11. Zuo W, Kwok H (2021) Development of marine-derived compounds for cancer therapy. Mar Drugs 19(6):342
12. Sheng R, Qin Z (2019) History and current status of autophagy research. Autophagy: biology and diseases. Springer, Singapore, pp 3–37
13. Frake RA, Rubinsztein D (2016) Yoshinori Ohsumi's Nobel prize for mechanisms of autophagy: from basic yeast biology to therapeutic potential. J R Coll Physicians Edinb 46(4):228–233
14. Shi S et al (2018) Effects of tetrahedral DNA nanostructures on autophagy in chondrocytes. Chem Commun 54(11):1327–1330
15. Czaja MJ (2016) Function of autophagy in nonalcoholic fatty liver disease. Dig Dis Sci 61(5):1304–1313
16. Shi Q et al (2020) Mechanisms of action of autophagy modulators dissected by quantitative systems pharmacology analysis. Int J Mol Sci 21(8):2855
17. Campos-Blázquez, J. et al. Relationship between ROS, autophagy, and cancer. 2022
18. Cui B, Yu J (2018) Autophagy: a new pathway for traditional Chinese medicine. J Asian Nat Prod Res 20(1):14–26
19. Xiao Z et al (2020) Autophagy promotion enhances the protective effect of Morroniside on human OA chondrocyte. Biosci Biotechnol Biochem 84(5):989–996
20. Yang A, Hacheney I, Wu Y (2017) Semisynthesis of autophagy protein LC3 conjugates. Bioorg Med Chem 25(18):4971–4976
21. Suzuki H et al (2017) Structural biology of the core autophagy machinery. Curr Opin Struct Biol 43:10–17
22. Su R et al (2017) Particulate matter exposure induces the autophagy of macrophages via oxidative stress-mediated PI3K/AKT/mTOR pathway. Chemosphere 167:444–453
23. Lin C et al (2016) Honokiol induces autophagic cell death in malignant glioma through reactive oxygen species-mediated regulation of the p53/PI3K/Akt/mTOR signaling pathway. Toxicol Appl Pharmacol 304:59–69
24. Le Sage V et al (2016) Adapting the stress response: viral subversion of the mTOR signaling pathway. Viruses 8(6):152
25. Dikic I, Elazar Z (2018) Mechanism and medical implications of mammalian autophagy. Nat Rev Mol Cell Biol 19(6):349–364
26. Amaravadi R, Kimmelman AC, White E (2016) Recent insights into the function of autophagy in cancer. Genes Dev 30(17):1913–1930
27. Kocak M et al (2021) Targeting autophagy in disease: established and new strategies. Autophagy 18:1–23
28. El-Shafey ES, Elsherbiny ES (2019) Possible selective cytotoxicity of vanadium complex on breast cancer cells involving pathophysiological pathways. Anti-Cancer Agents Med Chem (formerly current medicinal chemistry-anti-cancer agents) 19(17):2130–2139
29. Sutradhar M et al (2019) Antiproliferative activity of heterometallic sodium and potassium-dioxidovanadium (V) polymers. J Inorg Biochem 200:110811
30. Kowalski S et al (2019) New oxidovanadium (IV) coordination complex containing 2-methylnitrilotriacetate ligands induces cell cycle arrest and autophagy in human pancreatic ductal adenocarcinoma cell lines. Int J Mol Sci 20(2):261
31. Kowalski S et al (2017) Selective cytotoxicity of vanadium complexes on human pancreatic ductal adenocarcinoma cell line by inducing necroptosis, apoptosis and mitotic catastrophe process. Oncotarget 8(36):60324
32. Huang Y et al (2018) Vanadium (IV)-chlorodipicolinate alleviates hepatic lipid accumulation by inducing autophagy via the LKB1/AMPK signaling pathway in vitro and in vivo. J Inorg Biochem 183:66–76
33. Machado PA et al (2017) VOSalophen: a vanadium complex with a stilbene derivative—induction of apoptosis, autophagy, and efficiency in experimental cutaneous leishmaniasis. JBIC J Biol Inorg Chem 22(6):929–939
34. Walker CL et al (2012) Systemic bisperoxovanadium activates Akt/mTOR, reduces autophagy, and enhances recovery following cervical spinal cord injury. PLoS One 7(1):e30012
35. Wu Y et al (2014) Sodium orthovanadate inhibits growth of human hepatocellular carcinoma cells in vitro and in an orthotopic model in vivo. Cancer Lett 351(1):108–116
36. Lin F, Wang R (2010) Systematic derivation of AMBER force field parameters applicable to zinc-containing systems. J Chem Theory Comput 6(6):1852–1870
37. Kashefolgheta S, Verde AV (2017) Developing force fields when experimental data is sparse: AMBER/GAFF-compatible parameters for inorganic and alkyl oxoanions. Phys Chem Chem Phys 19(31):20593–20607
38. Islam M et al (2016) Interactions of hydrogen with the iron and iron carbide interfaces: a ReaxFF molecular dynamics study. Phys Chem Chem Phys 18(2):761–771
39. Rogacka J et al (2019) Intermediate states approach for adsorption studies in flexible metal–organic frameworks. Phys Chem Chem Phys 21(6):3294–3303
40. Hu L, Ryde U (2011) Comparison of methods to obtain force-field parameters for metal sites. J Chem Theory Comput 7(8):2452–2463
41. Taylor-Edinbyrd K, Li T, Kumar R (2017) Effect of chemical structure of S-nitrosothiols on nitric oxide release mediated by the copper sites of a metal organic framework based environment. Phys Chem Chem Phys 19(19):11947–11959
42. Prandi IG et al (2016) Combining classical molecular dynamics and quantum mechanical methods for the description of electronic excitations: the case of carotenoids. J Comput Chem 37(11):981–991
43. Álvarez L et al (2010) Comparison of the coordination capabilities of thiodiacetate and oxydiacetate ligands through the X-ray characterization and DFT studies of [V (O)(tda)(phen)]· 4H2O and [V (O)(oda)(phen)]· 1.5 H2O. Polyhedron 29(16):3028–3035
44. Kaur N et al (2016) Spin inversion phenomenon and two-state reactivity mechanism for direct benzene hydroxylation by V4O10 cluster. J Phys Chem A 120(48):9588–9597
45. Kaur N, Gupta S, Goel N (2017) Enantioselective synthesis of sulfoxide using an SBA-15 supported vanadia catalyst: a computational elucidation using a QM/MM approach. Phys Chem Chem Phys 19(36):25059–25070
46. Frisch MJ et al (2013) Gaussian 09, Revision E.01. Gaussian, Inc., Wallingford CT

47. Neese F (2017) Software update: the ORCA program system, version 4.0. Wiley Interdisciplinary Reviews: Computational Molecular. Science 8(1):e1327
48. Cárdenas G et al (2021) A force field for a manganese-vanadium water oxidation catalyst: redox potentials in solution as showcase. Catalysts 11(4):493
49. Cornell WD et al (2002) Application of RESP charges to calculate conformational energies, hydrogen bond energies, and free energies of solvation. J Am Chem Soc 115(21):9620–9631
50. Seminario JM (1996) Calculation of intramolecular force fields from second-derivative tensors. Int J Quantum Chem 60(7):1271–1277
51. Mayne CG et al (2013) Rapid parameterization of small molecules using the force field toolkit. J Comput Chem 34(32):2757–2770
52. Humphrey W, Dalke A, Schulten K (1996) VMD: visual molecular dynamics. J Mol Graph 14(1):33–38
53. Case DA et al (2021) Amber 2021. University of California, São Francisco
54. Salmaso V, Moro S (2018) Bridging molecular docking to molecular dynamics in exploring ligand-protein recognition process: an overview. Front Pharmacol 9:923
55. Pereira AF, Prandi IG, Ramalho TC (2021) Parameterization and validation of a new force field for Pt (II) complexes of 2-(4′-amino-2′-hydroxyphenyl) benzothiazole. Int J Quantum Chem 121(6):e26525
56. Cousins KR (2011) Computer review of ChemDraw Ultra 12.0. J Am Chem Soc 133:8388
57. Wang J et al (2004) Development and testing of a general amber force field. J Comput Chem 25(9):1157–1174
58. Sebesta F et al (2016) Estimation of transition-metal empirical parameters for molecular mechanical force fields. J Chem Theory Comput 12(8):3681–3688
59. D'Angelo ND et al (2011) Discovery and optimization of a series of benzothiazole phosphoinositide 3-kinase (PI3K)/mammalian target of rapamycin (mTOR) dual inhibitors. J Med Chem 54(6):1789–1811
60. Waterhouse A et al (2018) SWISS-MODEL: homology modelling of protein structures and complexes. Nucleic Acids Res 46(W1):W296–W303
61. Martínez L, Andreani R, Martínez JM (2007) Convergent algorithms for protein structural alignment. BMC Bioinformatics 8(1):1–15
62. Thomsen R, Christensen MH (2006) MolDock: a new technique for high-accuracy molecular docking. J Med Chem 49(11):3315–3321
63. Gurumoorthy P, Mahendiran D, Rahiman AK (2016) Theoretical calculations, DNA interaction, topoisomerase I and phosphatidylinositol-3-kinase studies of water soluble mixed-ligand nickel (II) complexes. Chem Biol Interact 248:21–35
64. Case DA et al (2005) The Amber biomolecular simulation programs. J Comput Chem 26(16):1668–1688
65. Arba M, Sufriadin M, Tjahjono DH (2020) Identification of phosphatidylinositol 3-kinase δ (PI3Kδ) inhibitor: pharmacophore-based virtual screening and molecular dynamics simulation. Indian J Chem 20(5):1070–1079
66. Farrokhzadeh A, Akher FB, Egan TJ (2021) Molecular mechanism exploration of potent fluorinated PI3K inhibitors with a triazine scaffold: unveiling the unusual synergistic effect of pyridine-to-pyrimidine ring interconversion and CF3 defluorination. J Phys Chem B 125(36):10072–10084
67. Jorgensen WL et al (1983) Comparison of simple potential functions for simulating liquid water. J Chem Phys 79(2):926–935
68. Ryckaert JP, Ciccotti G, Berendsen HJC (1977) Numerical integration of the cartesian equations of motion of a system with constraints: molecular dynamics of n-alkanes. J Comput Phys 23(3):327–341
69. Darden T, York D, Pedersen L (1993) Particle mesh Ewald: An N· log (N) method for Ewald sums in large systems. J Chem Phys 98(12):10089–10092
70. Izaguirre JA et al (2001) Langevin stabilization of molecular dynamics. J Chem Phys 114(5):2090–2098
71. Roe DR, Cheatham III TE (2013) PTRAJ and CPPTRAJ: software for processing and analysis of molecular dynamics trajectory data. J Chem Theory Comput 9(7):3084–3095
72. Hollingsworth SA, Dror RO (2018) Molecular dynamics simulation for all. Neuron 99(6):1129–1143
73. Santos LA, Prandi IG, Ramalho TC (2019) Could quantum mechanical properties be reflected on classical molecular dynamics? The case of halogenated organic compounds of biological interest. Front Chem 7:848
74. Tavares CA et al (2023) Molecular dynamics-assisted interaction of vanadium complex–AMPK: from force field development to biological application for Alzheimer's treatment. J Phys Chem B 127(2):495–504
75. Hyperchem (2001) Release 7.0 for Windows. Hypercube Inc., Gainesville FL USA
76. Pyper NC (2020) Relativity and the periodic table. Phil Trans R Soc A 378(2180):20190305
77. Sargsyan K, Grauffel C, Lim C (2017) How molecular size impacts RMSD applications in molecular dynamics simulations. J Chem Theory Comput 13(4):1518–1524
78. Del Río D et al (2003) Synthesis, molecular structure and properties of oxo-vanadium (IV) complexes containing the oxydiacetate ligand. Dalton Trans 9:1813–1820
79. Sprenger K, Jaeger V, Pfaendtner J (2015) The general AMBER force field (GAFF) can accurately predict thermodynamic and transport properties of many ionic liquids. J Phys Chem B 119(18):5882–5895
80. Rabet S, Raabe G (2022) Comparison of the GAFF, OPLSAA and CHARMM27 force field for the reproduction of the thermodynamics properties of furfural, 2-methylfuran, 2, 5-dimethylfuran and 5-hydroxymethylfurfural. Fluid Phase Equilib 554:113331
81. Jójárt B, Martinek T (2007) Performance of the general amber force field in modeling aqueous POPC membrane bilayers. J Comput Chem 28(12):2051–2058
82. Del Río D et al (2000) Synthesis, antiapoptotic biological activity and structure of an oxo–vanadium (IV) complex with an OOO ligand donor set. Inorg Chem Commun 3(1):32–34
83. Naqvi AAT et al (2018) Advancements in docking and molecular dynamics simulations towards ligand-receptor interactions and structure-function relationships. Curr Top Med Chem 18(20):1755–1768
84. Alonso H, Bliznyuk AA, Gready JE (2006) Combining docking and molecular dynamic simulations in drug design. Med Res Rev 26(5):531–568
85. Kaleağasioğlu F, A DM, Berger MR (2020) Multiple facets of autophagy and the emerging role of alkylphosphocholines as autophagy modulators. Front Pharmacol 11:547